M-Side Electron Transfer in Reaction Center Mutants with a Lysine near the Nonphotoactive Bacteriochlorophyll†

Christine Kirmaier,* Danielle Weems, and Dewey Holten*

Department of Chemistry, Washington University, St. Louis, Missouri 63130

Received April 13, 1999; Revised Manuscript Received June 8, 1999

ABSTRACT: We report the primary charge separation events in a series of *Rhodobacter capsulatus* reaction centers (RCs) that have been genetically modified to contain a lysine near the bacteriochlorophyll molecule, $BChl_M$, on the nonphotoactive M-side of the RC. Using wild type and previously constructed mutants as templates, we substituted Lys for the native Ser residue at position 178 on the L polypeptide to make the S(L178)K single mutant, the S(L178)K/G(M201)D and S(L178)K/L(M212)H double mutants, and the S(L178)K/G(M201)D/L(M212)H triple mutant. In the triple mutant, the decay of the photoexcited primary electron donor (P*) occurs with a time constant of 15 ps and is accompanied by 15% return to the ground state, 62% electron transfer to the L-side bacteriopheophytin, BPh_L, and 23% electron transfer to the M-side analogue, BPh_M. The data supporting electron transfer to the M-side include bleaching of the Q_X band of BPh_M at 528 nm and a spectrally and kinetically resolved anion band with a maximum at 640 nm assigned to BPh_M^-. The decay of these features and concomitant ∼20% decay of bleaching of the 850 nm band of P give a $P^+BPh_M^-$ lifetime on the order of 1−2 ns that reflects deactivation to give the ground state. These data and additional findings are compared to those from parallel experiments on the G(M201)D/L(M212)H double mutant, in which 15% electron transfer to BPh_M has been reported previously and is reproduced here. We also compare the above results with the primary electron-transfer processes in S(L178)K, S(L178)K/G(M201)D, and S(L178)K /L(M212)H RCs and with those for the L(M212)H and G(M201)D single mutants and wild-type RCs. The comparison of extensive results that track the primary events in these eight RCs helps to elucidate key factors underlying the directionality and high yield of charge separation in the bacterial photosynthetic RC.

The bacterial reaction center (RC)[1] is the membrane-bound pigment−protein complex in which a series of fast electron-transfer reactions initiate the conversion of light energy into chemical potential energy (*1*−*3*). RCs from the purple bacteria contain a dimer of bacteriochlorophyll (BChl) molecules (P), two monomeric BChls, two bacteriopheophytin (BPh) chromophores, two quinone (Q) molecules, and a non-heme iron (Figure 1) (*4*−*7*). These cofactors are embedded in a protein consisting of the L, M, and H polypeptides. Macroscopic C_2 symmetry exists for the arrangement of the cofactors and the L and M polypeptides. Upon absorption of light, P is raised to its excited singlet state (P*), which transfers an electron in about 4 ps to BPh_L, the BPh most closely associated with the L polypeptide. $BChl_L$ is intimately involved in this initial charge separation process. In keeping with a wide range of observations, this cofactor may function by parallel roles as an intermediary electron carrier forming $P^+BChl_L^-$ and as a superexchange mediator (*8*−*40*). $P^+BPh_L^-$ subsequently transfers an electron to the primary quinone (Q_A) in about 200 ps. The overall quantum yield of this charge separation process is ∼1. In wild-type RCs, $BChl_M$ and BPh_M appear to be nonfunctional. Understanding how electron transfer to this alternate chain of electron carriers is effectively suppressed relative to L-side charge separation continues to be a major issue in the field (*1*−*3*).

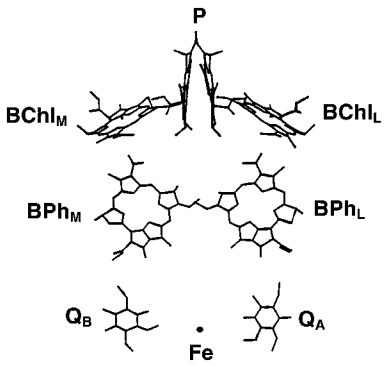

FIGURE 1: Arrangement of the RC cofactors as determined by the X-ray structures of RCs from *Rps. viridis* and *Rb. sphaeroides* (*4*−*7*).

The overall charge separation process in wild-type (wt) RCs described above is depicted in Figure 2a. The free energies of P* (∼1.4 eV), $P^+BPh_L^-$ (∼1.1 eV), and $P^+Q_A^-$ (∼0.6 eV) are known from experiments (*41*), although when initially formed $P^+BPh_L^-$ may lie even closer to P* (*24*, *42*). A growing body of experimental evidence (*10*−*26*) and several but not all electrostatic and other calculations (*8*, *9*, *35*, *42*−*48*) place $P^+BChl_L^-$ reasonably close to P*, and

† This work was supported by Grant MCB-9723008 from the National Science Foundation.

[1] Abbreviations: RC, reaction center; BChl, bacteriochlorophyll; P, dimeric BChl primary donor; BPh, bacteriopheophytin; Q, quinone; L and M, polypeptide subunits.

10.1021/bi9908585 CCC: $18.00
Published on Web 08/14/1999

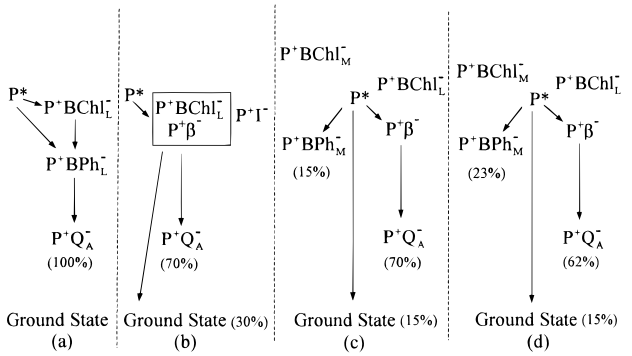

FIGURE 2: Schematic state diagram comparing the proposed free energy ordering of the states and the primary events in various RC types as summarized in Table 1. Note that the free energy gaps are not shown to scale and that the free energy of $P^+BChl_M^-$ relative to P* may be somewhat different than indicated. The box enclosing $P^+BChl_L^-$ and $P^+\beta^-$ in (b) indicates that in the simple beta-type RCs these states are thought to be very close in (free) energy and both contribute to the L-side intermediate P^+I^-. Their ordering may in fact be reversed ($P^+\beta^-$ the higher of the two) depending on the RC (the mutation and whether in *Rb. capsulatus* or *Rb. sphaeroides*). Processes that may occur with yields <10% are not shown [e.g., possible decay of $P^+\beta^-$ to the ground state in (c)].

probably below P*, as is indicated in Figure 2a. The L(M214)H *Rhodobacter sphaeroides* RC [and the analogous L(M212)H in *Rhodobacter capsulatus*] is a key mutant that indirectly indicates this close energy proximity (*19*−*21*). In this mutant, the native Leu at position 212 on the M polypeptide is replaced with His. (We will use *Rb. capsulatus* numbering throughout.) The L(M212)H mutation results in the incorporation of a BChl, denoted β, in place of the native BPh_L. RCs from two other *Rb. capsulatus* mutants, A(L124)H and F(L121)H/F(L97)V, also have this same non-native pigment content. Collectively, these RCs have been called "beta-type" RCs, and their primary electron-transfer events are depicted in Figure 2b. P* has a longer lifetime in beta-type RCs than in wt (∼8 ps versus ∼4 ps) and decays to form an intermediate denoted P^+I^- with a yield of ∼1 (*19*−*21*). This intermediate, thought to be an admixture of $P^+\beta^-$ and $P^+BChl_L^-$, decays in a few hundred picoseconds to give $P^+Q_A^-$ in ∼70% yield, with ∼30% of P^+I^- deactivating to the ground state. (The exact values depend on the specific mutant.) RCs that have been chemically treated to replace BPh_L with another tetrapyrrole pigment also exhibit these overall beta-type electron-transfer characteristics (*15*−*18*).

BChl is harder to reduce than BPh in vitro, and the same is true of the various tetrapyrroles that have been substituted into the BPh_L site (*15*, *17*, *49*). Thus, it has been proposed that the key to the altered photochemistry in the beta-type RCs is that $P^+\beta^-$ is at higher free energy than $P^+BPh_L^-$ in wt. This would place $P^+\beta^-$ closer to (and perhaps above) $P^+BChl_L^-$, thereby facilitating mixing between them (to produce P^+I^- as depicted in Figure 2b). Extensive measurements have been devoted to understanding the extent to which the mixing between $P^+BChl_L^-$ and $P^+\beta^-$ is quantum mechanical or thermal in nature. While the details are not fully elucidated and may vary in degree from one beta-type RC to another, a consistent explanation of the altered photochemistry is found in the role of $P^+BChl_L^-$ in driving rapid charge recombination that deactivates a portion of P^+I^- to the ground state with a time constant on the order of 1 ns. Qualitatively, this enhanced decay can be understood in terms of the small distance between the electron density on $BChl_L^-$ and the hole on P^+. Since $P^+BChl_L^-$ could effectively mix with $P^+\beta^-$ (or the corresponding states in chemically modified RCs) only if the two states are close in energy (or free energy depending on the mechanism), it is postulated that $P^+BChl_L^-$ lies slightly below P* (*16*−*21*).

We recently reported another RC that exhibits beta-type photochemistry (lengthened P* lifetime and branching at P^+I^- as in Figure 2b), although in this case the wt pigment content is retained (*22*). This RC is from the F(L121)D mutant, in which an Asp residue is placed close to ring V of BPh_L. The finding that this mutant exhibits beta-type photochemistry can be understood within the same basic framework described above. In particular, it is proposed that $P^+BPh_L^-$ lies at higher free energy in the F(L121)D mutant than in wt RCs due to an effect of the Asp at L121 making BPh_L to harder to reduce. This could result from either an ionized or a neutral Asp having a charge or polarity effect, respectively. Recent Raman measurements on the F(L121)D mutant suggest the Asp at L121 is (negatively) charged (*50*).

The G(M201)D/L(M212)H mutant is another RC in which we have introduced an Asp residue near a chromophore and observed a significant change in the primary events (*22*). In this double mutant, an Asp is placed near ring V of $BChl_L$ in the presence of the L(M212)H substitution that causes BPh_L to be replaced with β. Figure 2c summarizes the primary events in this mutant. P* has a longer lifetime (15 ps) than in either wt RCs (∼4 ps) or L(M212)H RCs (∼8 ps). P* decay is accompanied by 15% deactivation to the ground state, 70% electron transfer to the L-side, and 15% electron transfer to the normally inactive cofactor BPh_M. Subsequent electron transfer on the L-side to Q_A occurs with a time constant of 160 ps and a yield of >90%, giving an overall yield of $P^+Q_A^-$ approaching 70%. We have proposed that the Asp at M201 raises the free energy of $P^+BChl_L^-$, probably to above P*. In this way, a contribution of $P^+BChl_L^-$ to initial charge separation would be greatly diminished, no matter the mechanism (but probably more so if the two-step contribution is eliminated), thereby lengthening the P* lifetime and allowing some electron transfer to the M branch to take place. The proposed higher free energy of $P^+BChl_L^-$ in the G(M201)D/L(M212)H mutant also would decrease its involvement with $P^+\beta^-$ in P^+I^-. This explains the finding of a diminished pathway for P^+I^- charge recombination to the ground state and enhanced electron transfer to Q_A relative to the L(M212)H mutant (Figure 2b,c). As in the F(L121)D mutant, either a charged or neutral Asp at M201 could raise the free energy of $P^+BChl_L^-$. Recent Raman studies again support Asp M201 being (negatively) charged, at least at room temperature (*52*). The incorporation of the analogous Asp M203 in *Rb. sphaeroides* (*51*) and other mutations near $BChl_L$ also are thought to alter the redox properties of $BChl_L$ (and in some cases that of P as well) (*10*−*14*, *25*).

These mutants have provided insights into key factors impacting the directionality and yields of electron transfer in the RC by changing the relative free energies and contributions of the participating states. That free energy shifts are the primary (but probably not the sole) effects of these mutations is strongly supported by the consistency among (1) the effects on the various stages of charge

Table 1: Reaction Center Nomenclature and Summary Schemes

sample	nomenclature	scheme in Figure 1
wild type	wt	a
S(L178)K	K	a
G(M201)D	D	a
S(L178)K/G(M201)D	KD	a
L(M212)H	H	b
S(L178)K/L(M212)H	KH	b
G(M201)D/L(M212)H	DH	c
S(L178)K/G(M201)D/L(M212)H	KDH	d

separation in an individual mutant and (2) the variety of mutants that achieve similar or compensatory results. Electron transfer to the L- versus the M-sides in the RC may be substantially modulated by the relative free energies of $P^+BChl_L^-$ and $P^+BChl_M^-$, particularly if the former state is at lower free energy than the latter (and below P*) (*43*). This contribution to directionality, differences in the L- and M-side electronic couplings, and other asymmetries in the RC have been discussed (*23*, *35*, *36*, *43*−*48*, *53*−*65*). A change in the free energies of $P^+BChl_L^-$ and $P^+BChl_M^-$ may give a low yield of M-side electron transfer in mutants in which portions of the M and L polypeptides have been swapped (*63*).

To further explore the contribution of the relative free energies of $P^+BChl_L^-$ and $P^+BChl_M^-$ to directionality, we report here on a new series of mutants for which our goal is to increase the yield of electron transfer to the M branch. Using the G(M201)D/L(M212)H mutant as the starting point, we have made the further substitution of lysine for the native serine residue at position L178, which, similar to the Asp at M201 near $BChl_L$, puts this residue near ring V of $BChl_M$. However, Lys could have a dipole effect opposite to that induced by an Asp residue and, if ionized, would be positively charged. In this way, the S(L178)K mutation might lower $P^+BChl_M^-$ in free energy, thereby enhancing the participation of this state and increasing the yield of electron transfer to BPh_M. We will report here, as depicted in Figure 2d, that there is indeed a larger yield of $P^+BPh_M^-$ in the S(L178)K/G(M201D)/L(M212)H triple mutant (23%) compared to the G(M201)D/L(M212)H double mutant (15%).

To fully evaluate charge separation in the S(L178)K/G(M201)D/L(M212)H RC, we have constructed the S(L178)K mutation alone and with G(M201)D and L(M212)H in double mutants. These constructs were made so that we could compare parallel results on a complete series of RCs that contain all combinations of the mutations at these sites. Table 1 lists the eight RCs studied here along with the nomenclature that we will adopt from this point on. Thus, the triple mutant will be simply denoted by KDH for the amino acid symbols corresponding to the three introduced mutations, the S(L178)K single mutant by K, the L(M212)H single mutant by H, and so on. Thus, in addition to the KDH mutant, we report the primary events in the K, KH, and KD mutants, as well as new studies (higher signal to noise) on the D, H, DH, and wt RCs. Collectively, this series, and the KDH mutant in particular, brings new insights into the unidirectionality of electron transfer in the wt RC and key factors that impact the relative rates of the charge separation and charge recombination reactions that compete at each stage of the primary events.

EXPERIMENTAL PROCEDURES

The Lys mutation at L178 was obtained by oligonucleotide-mediated site-directed mutagenesis using an oligo that changed the native Ser codon AGC for amino acid L178 to AAG for Lys. The oligo contained two additional silent mutations: a change at L175 of CTG to CTT (both codons for Leu) and at L177 of ATC to ATT (both codons for Ile). The change at L175 introduces a *Bst*XI restriction enzyme site, and that at L177 introduces a recognition site for the enzyme *Mse*I. Both of these were used for screening purposes. These mutations in the L-gene were verified by dideoxy DNA sequencing before the gene was assembled into the final pU2924 plasmid that contains the RC *puf* operon. They were subsequently reverified by isolating and deconstructing the plasmid DNA from the *Rb. capsulatus* K mutant and resequencing the L-gene. The KH, KD, and KDH mutants were constructed by simple cloning. In each case, we took our previously constructed pU2924 vector containing the M-gene H, D, or DH mutations, respectively, and spliced in the *Kpn*I−*Bam*HI L-gene fragment having the Lys mutation at L178. All other details of the plasmids and procedures have been described elsewhere (*21*−*23*, *66*).

Residue L178, by which we introduce a Lys near $BChl_M$, is not the C_2 symmetry analogue of M201. That residue is L174. Simple substitution of Lys at L178 in the *Rb. sphaeroides* crystal structure coordinates (*4*) places its side chain nitrogen on average slightly closer to ring V of $BChl_M$ than would a Lys at L174. For Lys at L178 the distances include 4.0 Å to the ring V C_{10} carbonyl oxygen and 7.1 Å to the C_9 keto oxygen. These distances are larger overall than those estimated for the G(M201)D mutant between the two oxygens of Asp M201 to the ring V C_{10} carbonyl oxygen (3.4 and 4.5 Å) and to the C_9 keto oxygen (2.6 and 4.8 Å) of $BChl_L$. Of further note, a potential H-bond between Ser L178 and the $BChl_M$ ring IV propionate carbonyl oxygen is removed when Lys replaces the residue. This H-bond change is not expected to modulate the properties of $BChl_M$ since this C═O group is far removed from and not conjugated with the macrocycle, consistent with the results for the S(L178)K mutant (vide infra). Finally, we note that the closest distance between the side chain nitrogen of Lys L178 and P is over 12 Å.

RC isolation and purification followed standard procedures (*21*−*23*). One addition was a final cyt *c* column chromatography step (*67*). This additional step removes the cyt *c* oxidase that otherwise appears to copurify with the *Rb. capsulatus* RC protein to a varying extent from one preparation to another. We have used this step either in place of or in addition to a second round of standard DEAE chromatography to more easily achieve RC samples with A_{280}/A_{800} between 1.4 and 1.7. We have observed no differences in the time-resolved spectral data for RCs that have been purified with the cyt *c* column step versus those that have not. In all cases the final buffering solution for the RCs was 10 mM potassium phosphate, pH 7.6/0.05% LDAO/1 mM EDTA. Our standard isolation procedures yield RCs that are (>90%) depleted of Q_B, and this was verified to be the case here in flash photolysis experiments in which we examined the long time decay kinetics of P bleaching. These experiments utilized 30 ps, 532 nm, 1 mJ excitation flashes from an active/passive mode-locked Nd:YAG laser and

detection with an attenuated 850 nm diode laser and standard photomultiplier tube/amplifier/digitizer arrangement. In all cases, bleaching of the 850 nm band of P decayed >90% on the hundreds of milliseconds time scale (characteristic of $P^+Q_A^-$ charge recombination), with little if any evidence for decay on the time scale of seconds that would arise from $P^+Q_B^-$.

The initial electron-transfer reactions were studied by time-resolved absorption difference spectroscopy using either ~200 fs excitation flashes at 582 nm from a synchronously pumped dye laser system or ~130 fs flashes at 850 nm from a regeneratively amplified Ti:sapphire/OPA laser system (*23*, *68*). Both laser systems were operated at 10 Hz. The RC samples, ~2.5 mL total volume, were contained in an ice-cooled reservoir and flowed through a 2 mm path-length cell using a peristaltic pump. The temperature of the RCs was held near 10 °C using this arrangement. The laser excitation light was focused to ~1 mm and attenuated using neutral density filters so that 10−25% of the RCs in the excitation region were pumped on a given flash. Flowing ensured that fresh RCs were brought into the excitation region between flashes. The linearity of the conditions was verified by comparing the ΔA values when neutral density filters were added/removed from the pump light.

For the four RCs that contain β (H, KH, DH, and KDH), the transient difference spectra in the critical Q_X region were acquired under strictly the same conditions of the apparatus on matched samples with $A_{850} = 1.0$ in a 2 mm path-length cell. Hence, the raw spectral data are compared directly in Figure 6e−h. The Q_X data for the four RCs with native pigment content (wt, K, D, and KD) were acquired under very similar conditions of the apparatus on samples whose A_{850} varied from 0.8 to 1.1 in a 2 mm path-length cell. To facilitate comparisons of the amplitudes of the absorbance changes, and because the excitation conditions are very similar and linear, the data for the four RCs with native pigment content were scaled by small factors ranging from 0.9 to 1.25. In particular, the Q_X region data for these RCs (Figure 6a−d) have been scaled so that their integrated bleaching near 600 nm in the P* spectra is the same as for the H, KH, DH, and KDH RCs (Figure 6e−h). In this way, the spectra for the eight samples reflect the same initial concentration of P*. Whatever small factor was needed to achieve this P* normalization for a particular RC (wt, K, D, or KD), the same factor was then applied to the $P^+BPh_L^-$ and $P^+Q_A^-$ spectra for that sample. When the P* spectra were so normalized, the integrated bleaching of the BPh_L Q_X band in the spectrum of state $P^+BPh_L^-$ was found to be the same for the four RCs with native pigment content, reflecting the linearity of the conditions and the consistency of the data.

RESULTS

Ground-State Absorption Spectra. Figure 3 shows the 77 K ground-state absorption spectra of all eight RCs studied here. The top four spectra are for RCs that have wild-type pigment content (two BPhs and four BChls), and the bottom four spectra are for RCs that have the His mutation at M212 yielding β in place of BPh_L (one BPh and five BChls). Each of the top four spectra has a distinct pair of features, one near 530 nm and the other near 545 nm, that are assigned as

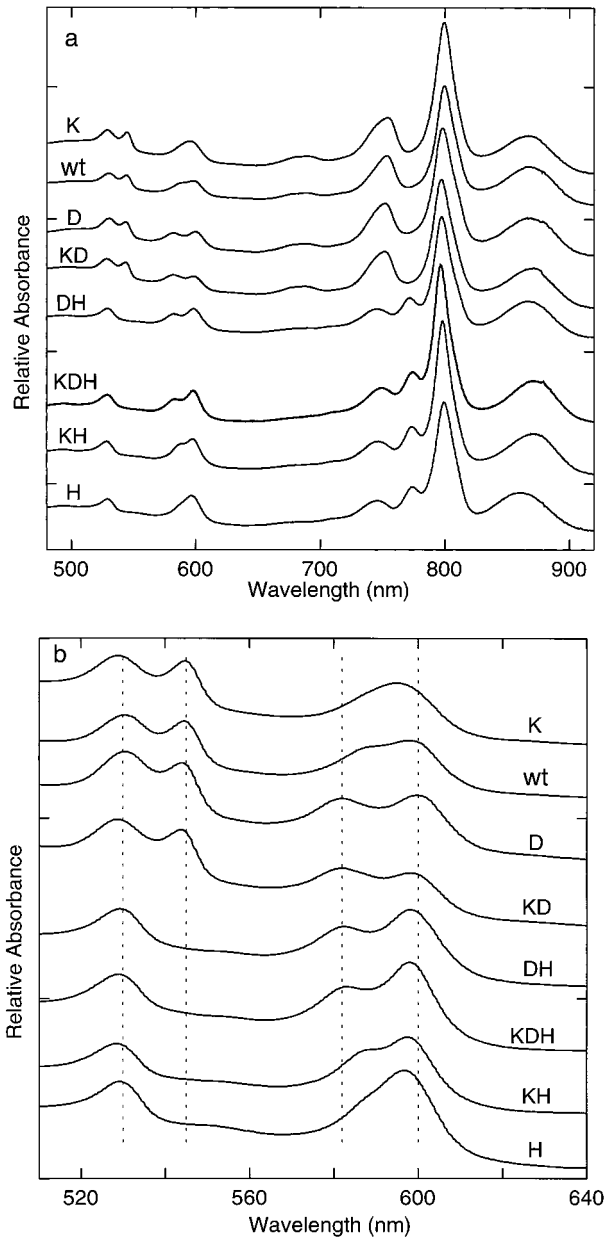

FIGURE 3: Ground-state absorption spectra of mutant and wild-type RCs in 60% glycerol/40% buffer (v/v) at 77 K. Panel b shows an expanded view of the Q_X region with dotted lines at 530, 545, 582, and 600 nm given for reference.

the Q_X bands of BPh_M and BPh_L, respectively. The four lower spectra have only the 530 nm Q_X band of BPh_M. In each of the latter spectra, the Q_X band of the β pigment is not distinctly resolved from that of the other BChls (570−620 nm), although in comparing the spectra of wt and H, it appears that this band lies near 595 nm at low temperature. The Q_Y band maximum of the β pigment is partially resolved near 780 nm for all four mutants that contain His at M212. Pigment extractions have been reported previously on the H and DH *Rb. capsulatus* mutants and the analogous *Rb. sphaeroides* L(M214)H mutant (*19*, *21*). We did not perform pigment extractions on the new series of mutants having Lys at L178 since no change in pigment content is expected. In this regard, the ground-state spectra provide clear evidence that the K and KD mutants have wt pigment content and that in the KH and KDH mutants BPh_L is replaced by β, as expected.

Another subfamily has members that contain the D mutation at M201 (D, KD, DH, and KDH RCs). The corresponding spectra are the middle four in Figure 3. The KD and KDH mutants both exhibit the partially resolved maximum at 582 nm that we reported previously for the D and DH mutants and suggested to be the blue-shifted position of the Q_X band of $BChl_L$ owing to the effect of Asp M201 near this cofactor (*22*, *23*). In contrast to the clear and consistent effect that the Asp at M201 has in all four mutants, there is no unambiguous effect of the Lys at L178 on the absorption spectrum. For example, in comparing the top two traces in Figure 3b, there seems to be a coalescing in the K mutant of the doublet of peaks observed at 588 and 600 nm in the wt spectrum. However, it should be noted that the extent of resolution of the two maxima in the wt spectra differs somewhat with conditions. Little evidence for a clear spectral effect of the Lys residue is apparent in comparing in turn the pairs D with KD, DH with KDH, and H with KH (Figure 3b). The H single mutant shows an asymmetrical band with a maximum peak at 595 nm and a shoulder at 588 nm. The shoulder is more pronounced in the KH mutant, but this is a subtle change at best given the complex nature of the RC spectrum in this region and given the similarity of the KH and wt spectra. A smaller effect of the K versus D mutation on the optical spectra may reflect the greater distance (or different orientation) of the Lys with respect to $BChl_M$ than the Asp to $BChl_L$ or differences in ionization states of these two residues.

Transient Absorption Spectra and Kinetics. The results of subpicosecond resolution transient absorption experiments are presented for all eight RCs in the following order: (1) in the 800−950 nm region encompassing the long-wavelength absorption band of P, (2) in the 500−600 nm region encompassing the Q_X bands of the pigments, and (3) in the 600−720 nm region where the anions of BPh and BChl have pronounced absorption bands. The data are arranged in this manner so that the reader can easily compare the photoinduced spectral changes among the RCs. Since the data in an individual spectral window give direct insights into different aspects of one or more of the electron transfer events and the states involved, the reader will be referred to the appropriate summary schemes in Figure 2. Using this bank of results as a framework, the Discussion section will focus largely on the KDH mutant to unify the key findings and conclusions.

P Bleaching and Stimulated Emission for RCs with Native Pigment Content. Representative transient absorption spectra in the region of the long-wavelength absorption band of P are shown in Figure 4 for the K and KD mutants. Formation of P* results in P bleaching near 850 nm (solid spectra at 0.3 ps). Stimulated emission from P* is manifested in these spectra as an additional trough on the red side of the 850 band, extending from near 850 nm to past 950 nm (compare with spectra at the longer times). The stimulated emission decay profiles were fit to a single exponential plus a constant (not shown) for seven 10 nm intervals between 870 and 940 nm. The resulting average P* lifetime for both RCs (and for similar experiments on D and wt RCs) is given in Table 2. The value for the K mutant is essentially the same as in wt RCs (∼4.5 ps), while the lifetimes for the D and KD mutants are slightly longer (∼8 ps). A value of ∼9 ps is found for the analogous *Rb. sphaeroides* G(M203)D mutant (*51*).

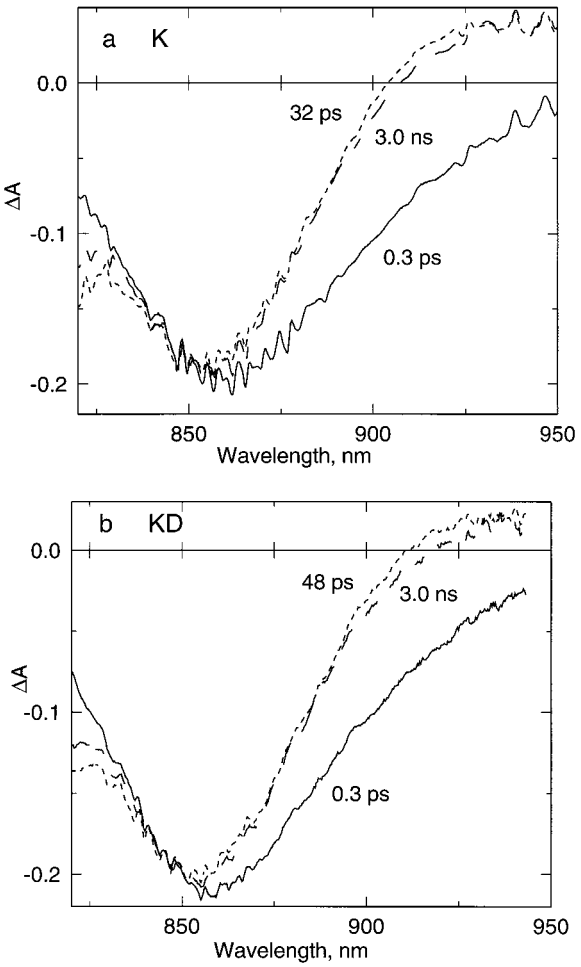

FIGURE 4: P-region transient absorption difference spectra of RCs from the (a) K and (b) KD mutants, taken at the times indicated following excitation with 0.2 ps flashes at 582 nm. See Table 2 for the P* lifetimes obtained from these data.

Table 2: Lifetimes for Samples Containing BPh_L[a]

sample	stimulated emission decay P* lifetime (ps)	BPh_L Q_X bleaching: appearance P* lifetime (ps)	BPh_L Q_X bleaching: decay $P^+BPh_L^-$ lifetime (ps)	anion absorption decay $P^+BPh_L^-$ lifetime (ps)
wt	4.3 ± 0.4	4.3 ± 0.3	160 ± 10	170 ± 10
K	4.7 ± 0.5	4.6 ± 0.4	170 ± 10	160 ± 10
D	7.6 ± 0.7	7.4 ± 0.4	160 ± 10	nm[b]
KD	8.1 ± 1.0	7.7 ± 0.5	160 ± 10	180 ± 20

[a] All data were taken at room temperature. The lifetimes are average values determined across the respective regions: stimulated emission (870−940 nm), BPh_L Q_X bleaching (535−545 nm), and BPh_L^- absorption (610−710 nm). [b] Not measured.

Following decay of P*, the true shape of the bleaching of the absorption band of the dimer is revealed in the two longer time spectra shown in Figure 4. The intermediate time spectra (32 and 48 ps) show data acquired at a delay corresponding to several P* lifetimes and can be assigned to state $P^+BPh_L^-$ on the basis of data in other regions. The spectra at 3 ns similarly can be ascribed to $P^+Q_A^-$ (vide infra). On the blue side of the P band (840−850 nm, where stimulated emission does not contribute), the magnitude of the bleaching is constant from the initial formation of P* to past 3 ns. Identical results have been reported previously for the D mutant (*11*) and are routinely obtained for wt RCs and

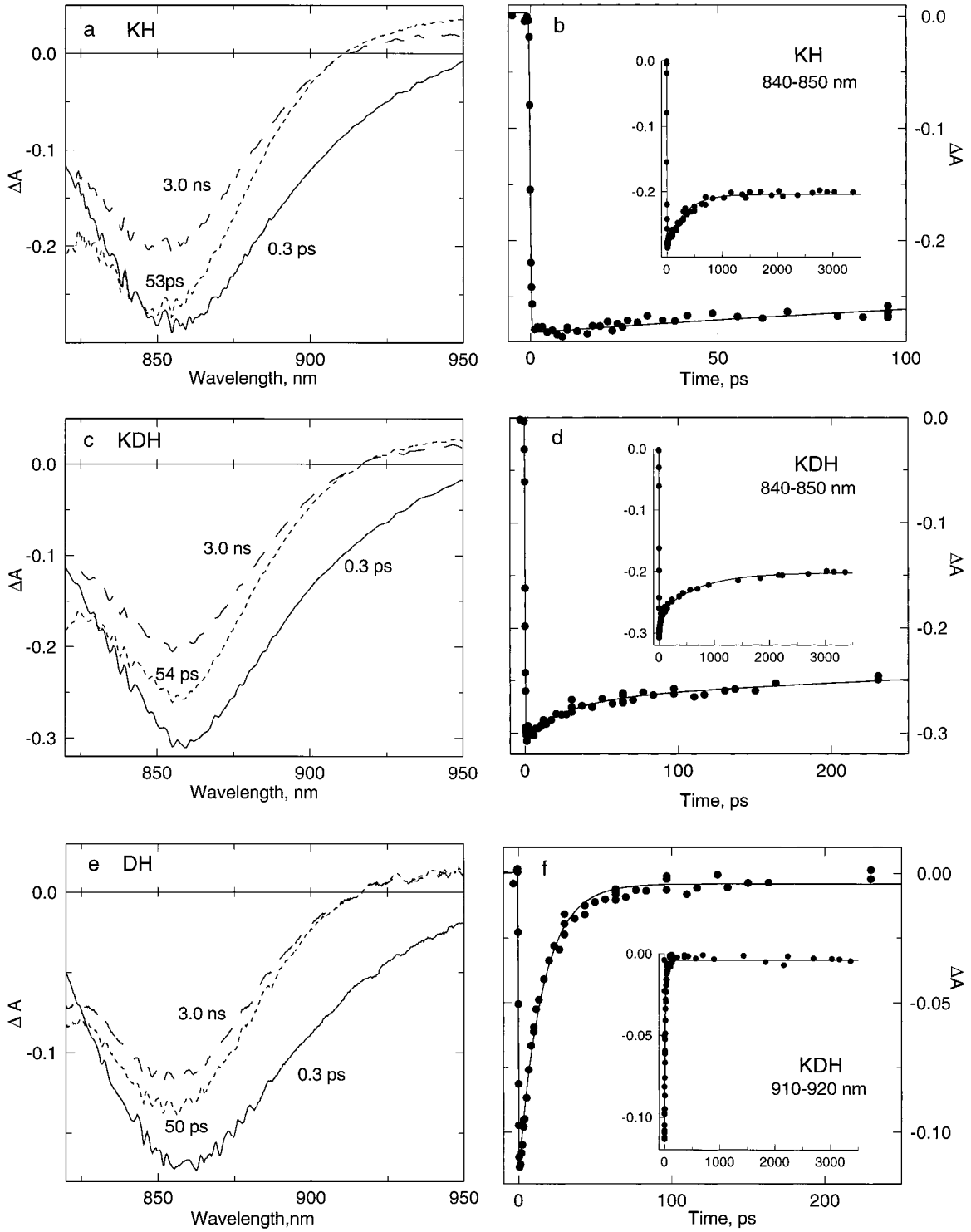

FIGURE 5: Transient absorption difference spectra of RCs from the (a) KH, (c) KDH, and (e) DH mutants, taken at the times indicated following excitation with 0.2 ps flashes at 582 nm. Representative kinetic data and fits are given in (b) for the KH and (d) and (f) for the KDH mutants. The insets show the complete data sets and fits, and the main figures show the first 100−200 ps. For the KH mutant in (b) the solid line is a fit of the data between 840 and 850 nm to the sum of an instrument function plus a single exponential plus a constant. For the KDH mutant in (d) the solid line is a fit of the data between 840 and 850 nm to the sum of the same instrument function plus two exponentials plus a constant. In (f) the stimulated emission data for the KDH mutant between 910 and 920 nm are fit to the instrument function plus a single exponential plus a constant. See Table 3 for the values of the time constants.

ascribed to a yield of ∼1 for the charge separation sequence $P^* \rightarrow (P^+BChl_L^-) \rightarrow P^+BPh_L^- \rightarrow P^+Q_A^-$ (Figure 2a). The data in Figure 4 together with those in other spectral regions indicate that the same is true for the K and KD mutants.

P Bleaching and Stimulated Emission for RCs with BPh_L Replaced by β. Figure 5 shows the results of similar experiments in the near-infrared region on three RCs in which BPh_L is replaced by β as a result of the H mutation. Overall, electron transfer in the KH mutant is very similar to that reported previously for the H mutant (Figure 2b). The P* spectrum for this mutant at 0.3 ps (Figure 5a) is the same as that for wt and the K, KD, and D mutants and again shows

Table 3: Lifetimes for Samples Containing β in Place of BPh_L[a]

sample	stimulated emission decay P* lifetime (ps)	anion absorption decay P^+I^- lifetime (ps)	anion absorption decay $P^+BPh_M^-$ lifetime (ns)	P bleach decay P^+I^- lifetime (ps)	P bleach decay $P^+BPh_M^-$ lifetime (ns)
H	8.5 ± 0.8	230 ± 30	*b*	250 ± 40	*b*
KH	8.2 ± 0.8	250 ± 20	*b*	300 ± 40	*b*
DH	15 ± 2	150 ± 30	1.0 ± 0.4	*c*	*c*
KDH	15 ± 2	130 ± 30	0.9 ± 0.2	*c*	0.8 ± 0.2[c]

[a] All data were taken at room temperature. The lifetimes are average values determined across the respective regions: stimulated emission (910−920 nm), I^- absorption (600−720 nm), BPh_M^- absorption (weighted at 630−650 nm), and near-infrared P bleaching (840−850 nm). [b] Not observed. [c] It is unclear at present to what extent P^+I^- decay may be accompanied by P bleaching recovery in the DH and KDH mutants. For the KDH mutant the data were fit under the model that the P bleaching recovery on the long time scale is due solely to decay to the ground state of $P^+BPh_M^-$, giving the time constant shown. For the DH mutant kinetic measurements on this time scale were not made due to the smaller magnitude of the absorbance change.

Table 4: Estimated Yields of the Primary Processes[a]

sample	P* decay: decay to ground state	P* decay: electron transfer to L-side	P* decay: electron transfer to M-side	L-side $P^+BPh_L^-$ or P^+I^- decay[b]: decay to ground state	L-side $P^+BPh_L^-$ or P^+I^- decay[b]: electron transfer to Q_A
wt	0	1	0	0	1
K	0	1	0	0	1
D[c]	0	1	0	0	1
KD	0	1	0	0	1
H[d]	0	0.94	0.06	0.24	0.76
KH	0	0.90	0.10	0.24	0.76
DH[e]	0.15	0.70	0.15	≤0.1[e]	≥0.9[e]
KDH	0.15	0.62	0.23	≤0.1[e]	≥0.9[e]

[a] All data were taken at room temperature. Yields have an error of 5%. [b] The L-side intermediate is $P^+BPh_L^-$ in wt, K, D, and KD RCs and an admixture (P^+I^-) of $P^+\beta^-$ and $P^+BChl_L^-$ in H, KH, DH, and KDH RCs that is more substantially weighted to $P^+\beta^-$ in the latter two. [c] The results reproduce those obtained in ref *23*. [d] The results reproduced those obtained in ref *21*. [e] It is difficult to assess whether there is modest charge recombination of the L-side intermediate due to the fact that parallel charge recombination of the M-side state $P^+BPh_M^-$ also contributes to decay of P bleaching.

stimulated emission on the red side of the P bleaching. A fit of the stimulated emission decay at 910−920 nm to a single exponential plus a constant gives a P* lifetime of 8.2 ± 0.8 ps (Table 3). The amplitude of bleaching at 840−850 nm is the same in the spectra at 0.3 ps (P*) and 53 ps (P^+I^-; see Figure 2b and below). This result indicates that decay of P* in KH RCs proceeds without detectable deactivation to the ground state.

However, at 3 ns the bleaching of the P band in the KH mutant is reduced to 76% of its initial amplitude. This finding indicates that P^+I^- decays by 24% return to the ground state (Table 4). The other 76% affords $P^+Q_A^-$, with the latter state giving rise to the spectrum at 3 ns. A fit of the bleaching decay between 840 and 850 nm to a single exponential plus a constant gives a time constant of 300 ± 40 ps that can be assigned as the P^+I^- lifetime (Figure 5b and Table 3). Kinetic data between 850 and 910 nm (where both P* stimulated emission and ground-state bleaching contribute) were fit to the sum of two exponentials and a constant. These fits return time constants of 8 ± 1 ps for the short component (the P* lifetime) and 300 ± 50 ps for the long component (the P^+I^- lifetime). Both values are in agreement with those noted above at wavelengths where either P* stimulated emission or P bleaching contributes essentially exclusively. Overall, the data in Figure 5a,b clearly show that the primary events in the KH mutant are very similar to those found for the H and other beta-type single mutants (Figure 2b and Table 4).

Near-infrared spectral and kinetic data for the KDH mutant are given in Figure 5c,d,f. The results are generally similar to those for the DH mutant, but with a few important differences in detail. For comparison, data for the latter mutant at higher signal to noise than obtained previously (*18*), but giving the same results, are shown in Figure 5e. The 0.3 ps P* spectra for the KDH and DH mutants are similar to those for wt and the other mutants. Decay of stimulated emission (910−920 nm) gives a P* lifetime of 15 ± 2 ps (Figure 5f and Table 3). Disappearance of P* is accompanied by 15% decay of the P bleaching between 840 and 850 nm, reflecting this extent of deactivation to the ground state (Figure 5c,e). The remaining 85% of the decay of P* in the KDH and DH mutants can be ascribed, on the basis of the data in other spectral regions, to formation (in different amounts) of P^+I^- (L-side) and $P^+BPh_M^-$. The latter two states together give rise to the spectra at ∼50 ps in Figure 5c,e. Between ∼50 ps and 3 ns, there is a further 21% decrease in the bleaching of the long-wavelength absorption band of P (840−850 nm) in the KDH mutant, indicating further deactivation to the ground state. Again, similar behavior is found in the DH mutant although the magnitude of the decay of P bleaching between ∼50 ps and 3 ns is less (14%). The data between 840 and 900 nm for the KDH mutant were fit to a dual exponential plus a constant, as exemplified in Figure 5d. The fits gave time constants of 15 ± 2 ps for the shorter component and 0.8 ± 0.2 ns for the longer component (Table 3). The former is the same as the P* lifetime determined from stimulated emission decay. As we will develop below in conjunction with data in the other wavelength regions, we believe the longer component is associated not with electron transfer or charge recombination processes on the L-side of the RC but rather largely reflects charge recombination of $P^+BPh_M^-$ to the ground state.

Absorbance Changes in the Q_X Region for RCs with Native Pigment Content. Figure 6 shows transient difference spectra in the 500−630 nm region, which encompasses bleaching of the Q_X bands of the chromophores. The top four panels show the data for the four RCs that have wt pigment. The amplitudes of the spectra for the four RCs can be compared directly since they have been scaled (by small factors) to the same initial P* concentration (see Experimental Procedures). The P* spectra (short dashes) are characterized by bleaching of the Q_X band of P at 595 nm embedded on a featureless transient absorption. As P* decays, bleaching centered near 542 nm in the Q_X band of BPh_L develops due to the formation of $P^+BPh_L^-$. The spectra (solid) showing this feature were acquired at delay times equivalent to four to five P* lifetimes as appropriate for each RC. By 3 ns (long dashed lines), bleaching of the Q_X band of BPh_L has decayed completely as a result of the electron-transfer process $P^+BPh_L^- \rightarrow P^+Q_A^-$. Note that the same near unity yield of the charge separation sequence P* → ($P^+BChl_L^-$) → $P^+BPh_L^- \rightarrow P^+Q_A^-$ (Figure 2a and Table 4) for wt, K, D,

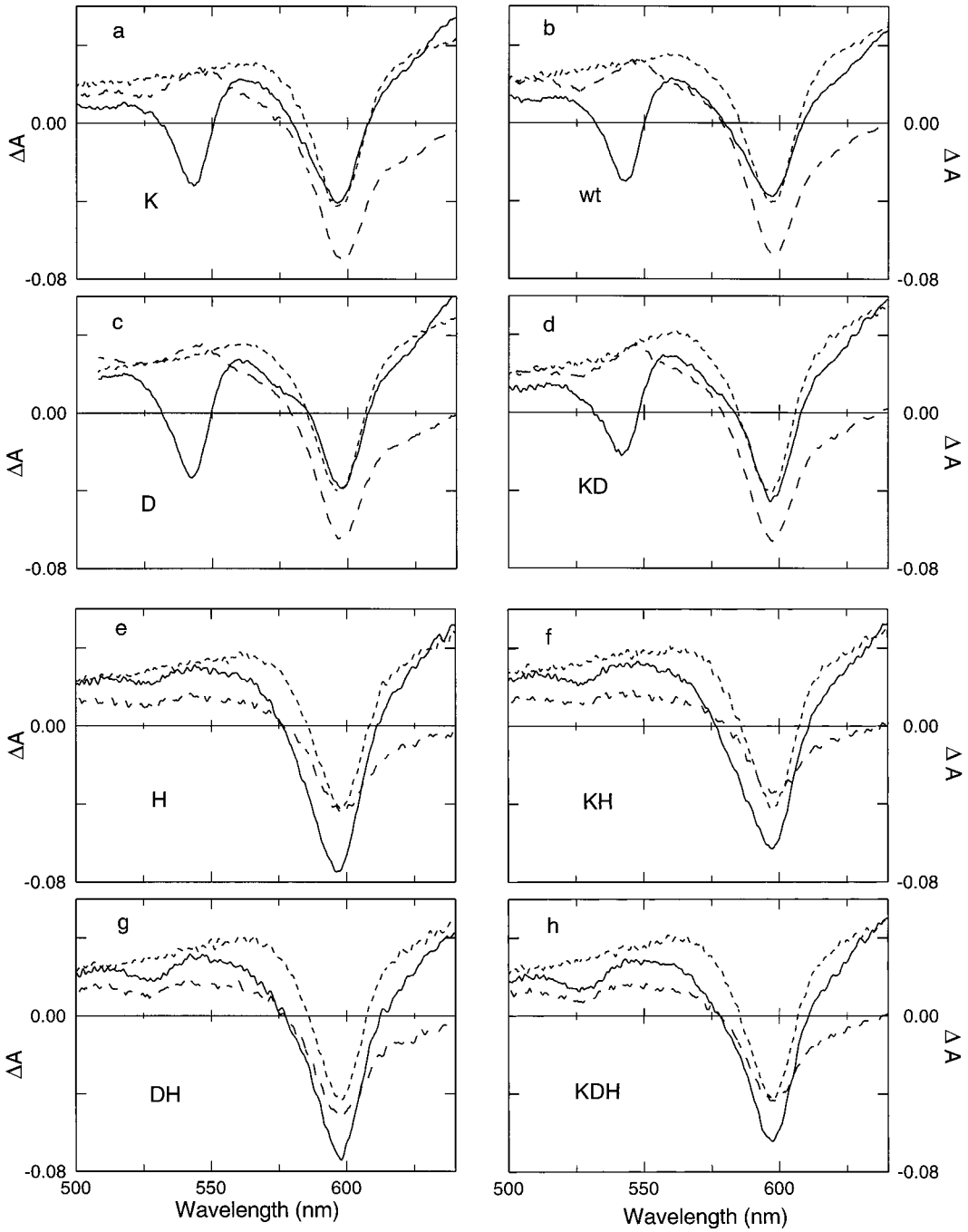

FIGURE 6: Transient absorption difference spectra encompassing the BPh and BChl Q_X bands in the eight samples under study here. The spectra were acquired using ~0.1 ps excitation flashes at 855 nm. In all cases the short-dashed lines are the P* spectra acquired immediately following excitation (~0.3 ps) and the long-dashed lines are the spectra taken at ~3 ns. The solid lines are the spectra acquired at delay times corresponding to three to five P* lifetimes as appropriate to each RC and are as follows: (a) 21 ps, (b) 18 ps, (c) 29 ps, (d) 28 ps, (e) 33 ps, (f) 35 ps, (g) 54 ps, and (h) 57 ps. The absorption changes in these spectra can be quantitatively compared from one RC to another (see Experimental Procedures).

and KD RCs is indicated by the following observations. (1) During the time course from 0.3 ps to 3 ns for each RC, the magnitude of the bleaching of the Q_X band of P near 600 nm remains essentially constant (relative to the opposing broad transient absorption that varies in amplitude). This finding coincides with the constant amplitude of bleaching in the near-infrared band of P for each RC. (2) The integrated BPh_L bleaching near 542 nm is essentially identical for the four RCs.

Representative kinetic data and fit for the formation and decay of the BPh_L Q_X band bleaching in the K mutant are given in Figure 7. The resulting time constants are included in Table 2 along with those for wt and the D and KD mutants (data not shown). For each of these four RCs, the rise time of the BPh_L bleaching (~4.5 ps for wt and K and ~8 ps for D and KD) is the same within error as the P* stimulated emission decay time (Table 2). The $P^+BPh_L^-$ lifetimes (determined from the decay of the bleaching) of ~160 ps for the K, KD, and D mutants are the same as for wt RCs (Table 2).

Absorbance Changes in the Q_X Region for RCs with BPh_L Replaced by β. Figure 6e−h shows Q_X data for the four

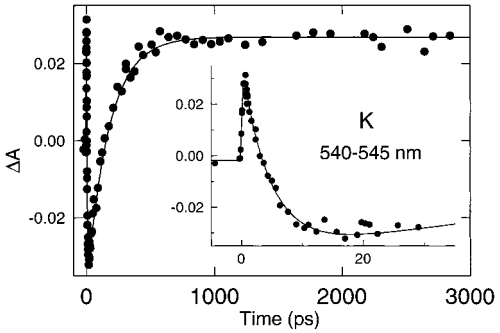

FIGURE 7: Kinetics of the appearance (inset) and decay (main figure) of bleaching of the BPh_L Q_X band at ~542 nm in RCs from the K mutant. These data were acquired using ~0.1 ps flashes at 855 nm. The main figure shows the complete data set, and the inset shows the first 35 ps. The solid lines are the fit to the sum of an instrument response plus two exponentials plus a constant. See Table 2 for the values of the time constants.

mutants that contain β as a result of the L(M212)H mutation. The spectral amplitudes for the different RCs are compared directly without scaling since the data were acquired under strictly the same conditions (see Experimental Procedures). The P* spectra (short dashed lines) are identical. The intermediate-time spectra shown at delay times corresponding to four or five P* lifetimes (solid) reflect the products of P* decay (Figure 2b−d). For each β-containing RC, the integrated bleaching near 600 nm at 25−50 ps is larger (more so on the blue side) than in the P* spectrum and larger than in the analogous spectra of the four RCs with native pigment content (Figure 6a−d). This increased bleaching occurs because electron transfer to the L-side causes reduction of β/$BChl_L$ (comprising I) and thus bleaching in the Q_X absorption bands of these cofactors, which partially overlap with the P bleaching.

The intermediate-time spectra also contain a small bleaching at 528 nm that differs in amplitude among the four β-containing mutants. In our previous work on the DH mutant, we assigned this feature to bleaching of the Q_X band of BPh_M due to the formation of $P^+BPh_M^-$. The yield was estimated to be 15% on the basis of comparison with the integrated amount of bleaching near 540 nm in wt RCs obtained under identical experimental conditions. This estimate is based on the reasonable assumption that the Q_X bands of the two BPhs have the same oscillator strength. The same yield is obtained here by comparing the integrated bleaching in DH with wt RCs (panels g and b of Figure 6) (or, equivalently, comparing with the K, D, or KD RCs.) The integrated area of the bleaching at 528 nm in the KDH mutant is ~50% larger than for the DH mutant (panels h and g of Figure 6), giving a $P^+BPh_M^-$ yield of 23% in the triple mutant. The H mutant has a much smaller BPh_M bleaching than in DH, as we reported previously, and the bleaching in the KH mutant is between that for the H and DH mutants. Comparisons with DH gives $P^+BPh_M^-$ yields of ~6% and ~10% in the H and KH mutants, respectively. Thus, the KH with H and KDH with DH pairs show parallel effects of Lys L178 on M-side transfer.

At 3 ns (long dashed lines), the bleaching near 530 nm is smaller in magnitude relative to 20−60 ps for all four β-containing RCs, clearly reflecting decay of $P^+BPh_M^-$. Estimates of 1−2 ns are obtained for the decay of 530 nm bleaching in the KDH and DH mutants (preliminary data, not shown), but these values carry large error bars due to the very small amplitudes of the absorption changes and the fact that the longest time point is ~3 ns. Nonetheless, such values are in reasonable agreement with the time constant of ~0.8 ns for the partial decay of P bleaching in the KDH mutant (Table 3), which carries a similar uncertainty due to the 3 ns time span of the data.

Anion Region Absorption Spectra and Kinetics. We turn last to the region of the spectrum where the anions of BPh and BChl have broad but characteristic absorption bands. Each RC shows the typical relatively featureless P* spectrum in this region. These data are not presented here; instead, we focus on the behavior after P* decay. Figures 8 and 9a show representative spectral and kinetic data for seven of the samples.

The spectrum at 25 ps for wt RCs is dominated by a broad band having a maximum near 665 nm characteristic of the BPh_L anion in the state $P^+BPh_L^-$. The time evolution across the entire 600−720 nm region is single exponential and gives a $P^+BPh_L^-$ lifetime of 170 ± 10 ps as indicated by the 640−650 nm data in Figure 8b. The spectrum at 700 ps (dashed), a delay corresponding to about four $P^+BPh_L^-$ lifetimes, is the same as that at 3 ns. These two spectra are characteristic of $P^+Q_A^-$ and include P bleaching near 600 nm, P^+ absorption near 710 nm, and ΔA ~0 between. Very similar spectra in the 600−720 nm region are found for the other RCs with native pigment content, namely the K and KD mutants (panels a and c of Figure 8, respectively) and D mutant (not shown). Likewise, the $P^+BPh_L^-$ lifetimes for these RCs are the same as that found for wt RCs (Table 2).

The H mutant is the template for RCs that contain β in place of BPh_L (Figure 8d). Following P* decay, the spectrum at 30 ps is broad with a maximum near 690 nm and a slightly weaker feature near 650 nm. This spectrum represents the transient intermediate P^+I^- that we have assigned as a thermal/quantum admixture of $P^+\beta^-$ and $P^+BChl_L^-$ (Figure 2b) (*19*−*23*). The decay kinetics measured across the entire region from 600 to 720 nm are well described by a single exponential function, as represented by the data at 640−650 nm in Figure 8d. The resulting P^+I^- lifetime is 230 ± 30 ps, which is in excellent agreement with the value of 250 ± 40 ps measured for the partial decay of P bleaching (Table 3). As in the case of the RCs with native pigment content (Figure 8a−c), the anion region spectrum of the H mutant at 700 ps is nearly identical to the spectrum at 3 ns, which can be assigned essentially exclusively to $P^+Q_A^-$.

The spectrum at 50 ps for the KDH mutant (Figure 9a) is generally similar to that shown at 30 ps for the H single mutant (Figure 8d). However, for the triple mutant, the shape of the spectrum at 700 ps is not only different from that at 50 ps but also different from the spectrum at 3 ns. In particular, the spectrum at 700 ps exhibits a weak but distinct band near 640 nm that is clearly larger than the absorption to longer wavelengths, between 680 and 720 nm. The opposite is true in the spectrum at 3 ns. As expected from these spectra, the time evolution of ΔA between 640 and 650 nm is clearly not well described by single exponential (Figure 9a, dashed line in main panel) but requires a fit to the sum of two exponentials plus a constant (solid line). Dual exponential fits (all parameters free) of the data between 630 and 660 nm return average time constants of 130 ± 30 ps and 0.9 ± 0.2 ns. At other wavelengths between 600 and

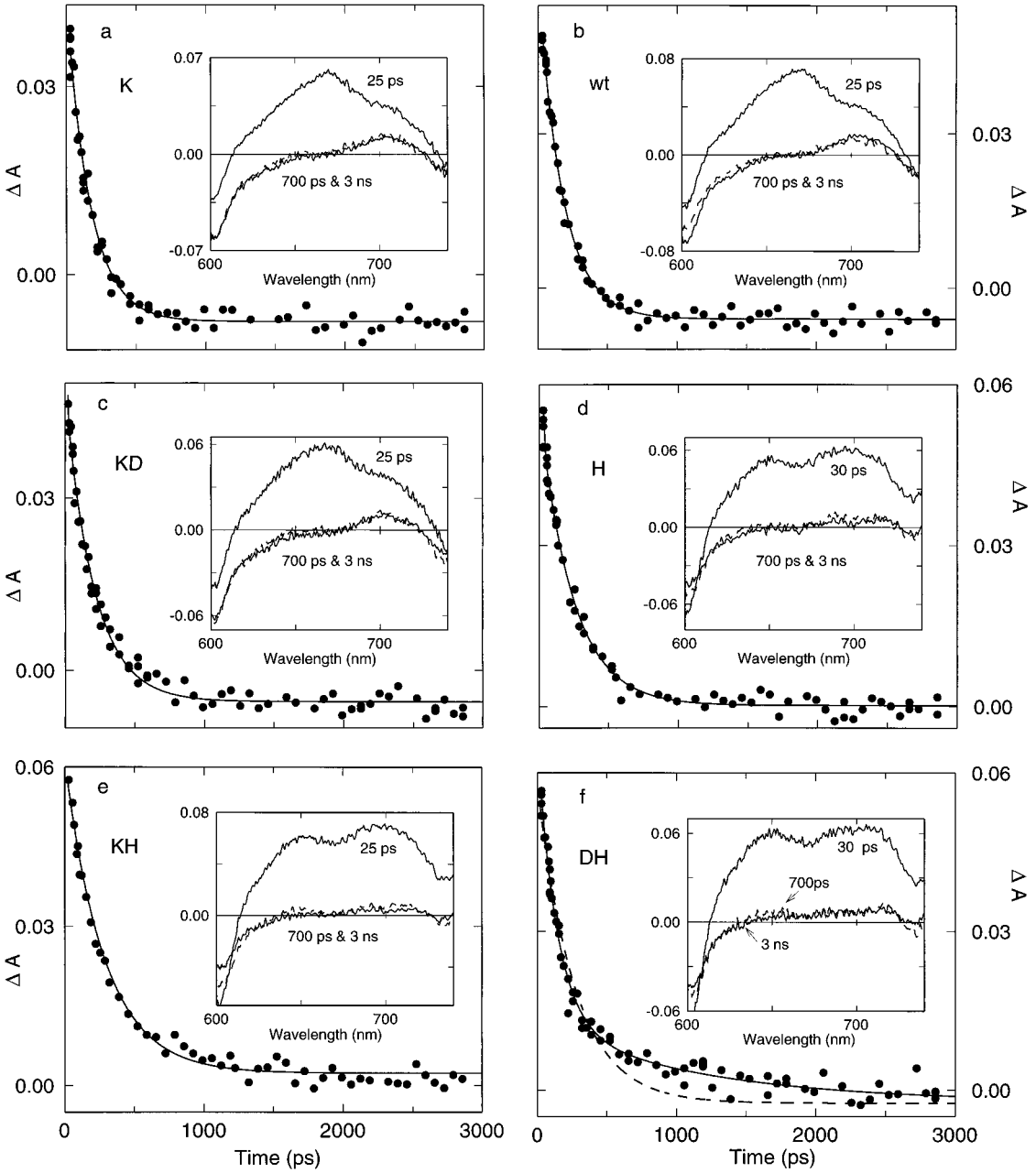

FIGURE 8: Transient absorption spectra (insets) and kinetics (main panels) taken in the region of the BPh and BChl anion bands using ~0.1 ps flashes at 855 nm. The kinetic data are for the transient absorption changes between 640 and 650 nm and have been deleted of points acquired during the excitation flash and P* lifetime. The fits shown as the solid lines are to a single exponential plus a constant for each of panels a−e. In (f) the solid line is a fit to the sum of two exponentials plus a constant, and the dashed line given for comparison is a fit to a single exponential with the constant (asymptote) fixed at the value returned from the dual exponential fit. See Tables 2 and 3 for the values of the time constants.

720 nm the contribution of the longer component is smaller than it is between 630 and 660 nm, but still present.

Since ΔA is near zero in the $P^+Q_A^-$ spectrum in this region, and since the time constants of the two kinetic components in the KDH mutant are well separated, the actual shapes of the spectra of the two components can be readily inferred from the raw spectra in Figure 9a. However, to better spectrally characterize the two anion region kinetic components, we calculated decay-associated spectra by holding the longer time constant fixed at 1 ns and refitting the data across this region in 25 intervals. The values returned from these fits for the shorter time constant ranged from 100 to 150 ps with an average value of 130 ps. Figure 9b shows a plot of the preexponential values with the triangles giving the ~130 ps component and the circles giving the (fixed) 1 ns component. As discussed above, the lifetime of the longer component could be somewhat larger than is indicated by these fits because the longest time point in the data set is ~3 ns, which is only a few multiples of the estimated lifetime. Essentially the same decay-associated spectra are obtained when the data are fit with the slower component held at 1.5 ns (results not shown). In this case an average lifetime of 150 ps is obtained for the shorter component. In this regard, the fits with the longer component fixed at 1.5 ns are not appreciably different by eye from the free fit shown in Figure 9a. However, visually worse fits and poorer correlation coefficients are found when the time constant of the longer component is fixed at a value larger than about 2 ns.

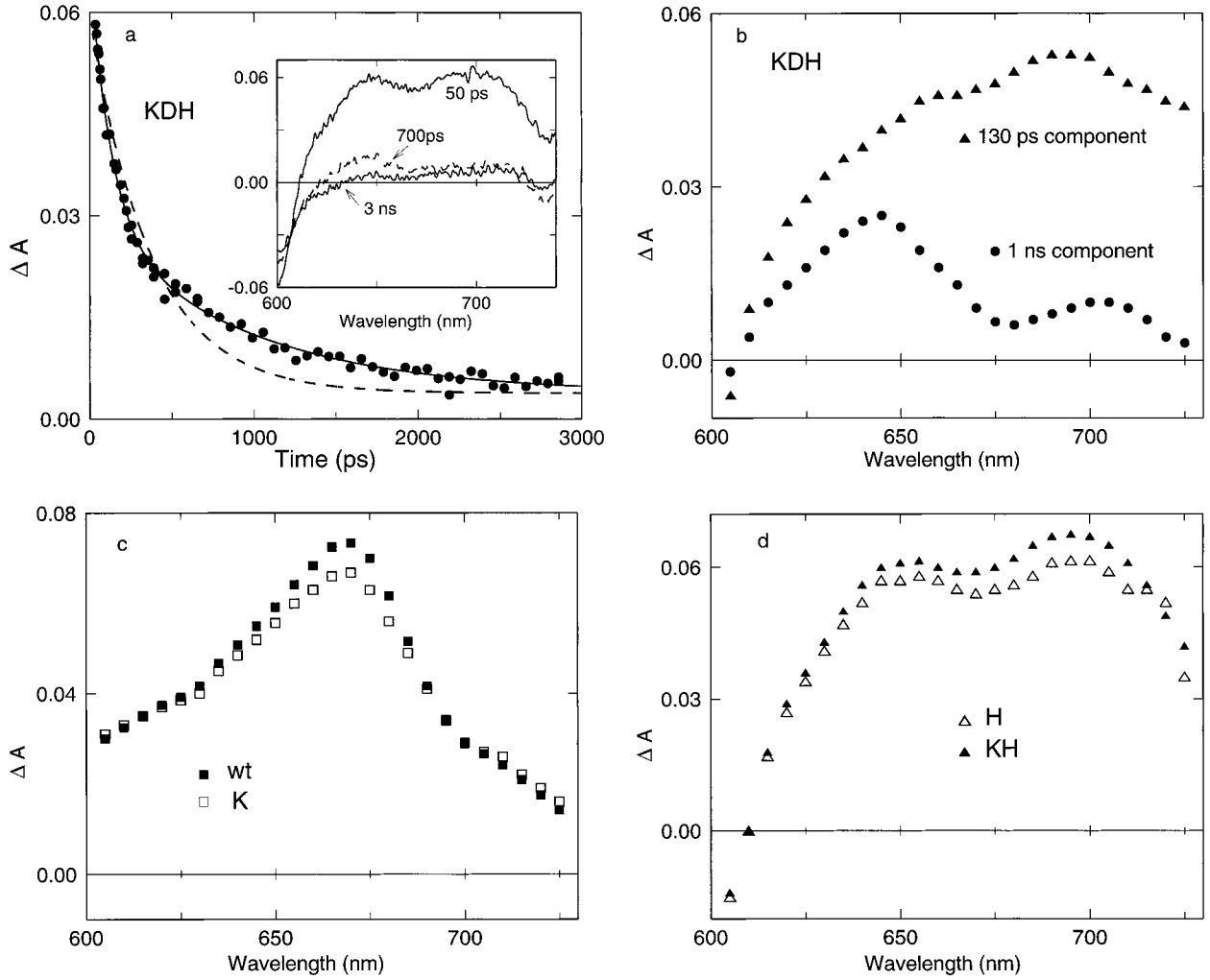

FIGURE 9: Panel (a) gives the spectral and kinetic data and fits for the KDH mutant presented in the same manner as for the DH sample in Figure 8f. Panel (b) shows the values of the preexponential factors of the dual exponential fits across the entire wavelength region for the KDH sample. Similar plots of the preexponential values from single exponential fits are given in (c) for wt and the K mutant and in (d) for the H and KH mutants (from data in Figure 8). See Table 3 for the values of the time constants for the KDH mutant and the text for further details.

It is clear that in the KDH mutant there are two spectrally and kinetically resolved anion-bearing intermediates contributing to the absorption changes between 600 and 720 nm, with lifetimes of ~130 ps and 1−2 ns. The shorter component has a spectrum with a maximum near 690 nm and a second feature of comparable amplitude near 650 nm (Figure 9b, triangles). This double-banded spectrum is similar to the spectrum assigned to the L-side P^+I^- intermediate in the H mutant (Figure 8d). The preexponentials from the single exponential fits of the H and KH mutants given in Figure 8d further demonstrate this point. The longer component in the KDH mutant has a spectrum with a maximum near 640 nm and a smaller feature near 700 nm (Figure 9b, circles). Again, for comparison, the preexponentials from the single exponential fits of wt and the K mutant are given in Figure 8c. Spectra identical to these are obtained for the KD and D mutants (data not shown). It is clear that the spectrum of the 1−2 ns component in the KDH mutant is distinct. We believe it is possible to assign this spectrum to $P^+BPh_M^-$ (see further discussion below), and when combined with the simultaneous presence of bleaching near 528 nm, we believe this assignment is unequivocal.

Finally, we consider the anion region data for the DH and KH mutants. As seen in Figure 8f, the 640−650 nm data in the DH mutant (acquired at higher signal to noise than previously) also deviate from single exponential behavior (dashed line). The data require a fit to a dual exponential plus a constant that returns time constants of 150 ± 30 ps and 1.0 ± 0.4 ns (solid line). As in the case of the KDH mutant, there is some uncertainty of the precise value of the longer component due to the limited time span of the data set. In the DH mutant, the amplitude of the longer component is clearly smaller than in the KDH mutant. This point can be seen visually by inspection of the kinetic and spectral data (Figure 8f versus Figure 9a). On a more quantitative level, when the data for matched samples are compared (giving P* spectra with identical amplitudes), the preexponential factor for the longer component at 640−650 nm is 1.6 times larger in the KDH mutant than in the DH mutant (0.025 versus 0.015). This factor is in excellent agreement with the ratio of 1.5 for the amplitudes of the BPh_M bleaching at 528 nm for the KDH versus DH mutants. Last, the data for the KH mutant shown in Figure 6e *may* deviate from single exponential, and there *may* be a hint of a 640 nm peak in the spectrum at 700 ps. On the basis of the Q_X region data discussed above, there may be ~6% and ~10% yields of M-side electron transfer in the H and KH mutants, respectively. However, unlike the DH and KDH mutants,

definitively ascertaining the presence of the longer lived anion component ($P^+BPh_M^-$) in the H and KH mutants is beyond our signal to noise.

DISCUSSION

We have previously shown that the primary electron transfer events are significantly altered when an Asp residue is placed near $BChl_L$ in a double mutant, G(M201)D/L(M212)H, that contains β in place of BPh_L (*23*) and, similarly, in the F(L121)D mutant where an Asp is introduced near BPh_L (*22*). One of the notable changes in the DH double mutant relative to the H single mutant is clear observation of electron transfer to the normally inactive M-side of the RC, forming $P^+BPh_M^-$ in 15% yield. We proposed that this M-side electron transfer results primarily from a slowing of initial electron transfer to the L-branch (increasing the P* lifetime) due to a higher free energy of $P^+BChl_L^-$ as caused by Asp M201. Using these results and interpretations as guides, we sought in the present study to directly facilitate electron transfer to the M-branch via free energy stabilization of $P^+BChl_M^-$ by placement of a Lys residue near $BChl_M$. The data collected above argue that the yield of $P^+BPh_M^-$ is increased to 23% in the KDH triple mutant and that the inherent lifetime of this state (i.e., its deactivation to the ground state) is on the order of 1−2 ns in this mutant. The strength of the conclusions concerning M-side electron transfer in the KDH and DH mutants is manifested in the qualitative and quantitative consistency of the spectral and kinetic data that probe $P^+BPh_M^-$. Additionally, there is agreement of the results on all eight RCs studied regarding the role of $P^+BChl_L^-$ in the competing charge separation versus charge recombination processes on the L-side. In the following discussion we highlight the underpinnings of these principal findings, focusing largely on the KDH and DH mutants.

M-Side versus L-Side Electron Transfer. One of the most compelling indications of M-side electron transfer in the KDH mutant is the presence of two spectrally and kinetically resolved components in the anion region (Figure 9a,b). Dual exponential behavior is also found for the DH mutant (Figure 8f). We assign the shorter lived (130−150 ps) component to the L-side intermediate P^+I^- and the longer lived (1−2 ns) component to the M-side state $P^+BPh_M^-$. It must be emphasized that the finding of two such components demonstrates that the spectral signatures we associate with $P^+BPh_M^-$ (640 nm anion absorption and 528 nm Q_X bleaching) cannot be ascribed instead to electrochromic or other effects accompanying charge separation on the L-branch. If this were true, the evolution with time of these spectral features would track kinetically the L-side events, which is not the case.

In further support of the assignment of the BPh_M anion band we show in Figure 10 the visible region difference spectra of BPh_L^- and BPh_M^- that were obtained in photochemical trapping experiments on wt *Rb. sphaeroides* RCs (*69*). It can be seen that the BPh_L^- spectrum has an anion band near 665 nm and bleaching of the BPh_L Q_X absorption near 540 nm. Both features are clearly at longer wavelengths than for BPh_M^-, which has an apparent anion band maximum near 625 nm and Q_X bleaching near 530 nm. These spectral differences between the two BPhs can be ascribed largely to the differences in hydrogen bonding to their ring V keto groups (*35*). The agreement between the characteristics of the BPh_M^- spectrum in Figure 10 and the transient spectrum of the long-lived component in our KDH and DH mutants is excellent considering that rigorously different species are being monitored. Specifically, the difference spectrum in Figure 10 is that of BPh_M^- whereas our experiments probe $P^+BPh_M^-$. In this regard, our $P^+BPh_M^-$ spectra contain bleaching due to P in the vicinity of 600 nm and a small absorption band near 710 nm that can be ascribed largely to P^+.

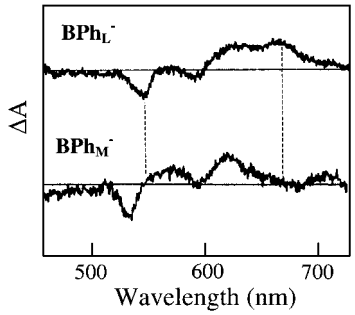

FIGURE 10: Spectra of the anions of BPh_L and BPh_M in wt *Rb. sphaeroides* RCs acquired in the phototrapping experiments from ref *69* and reproduced here with the kind permission of Dr. D. M. Tiede.

The internal consistency of these arguments extends further to the relative amplitudes of the spectral characteristics associated with $P^+BPh_M^-$ in KDH versus DH RCs. We have reported here that the magnitude of BPh_M Q_X bleaching near 530 nm is 1.5 times larger in KDH compared to DH, corresponding to relative yields of P* → $P^+BPh_M^-$ of 23% and 15%, respectively. Similarly, the slower component of the anion region decay near 640 nm in the triple mutant is larger than in the double mutant by essentially the same factor (1.6). Likewise, the slower components to the decay of the P bleaching in the KDH and DH RCs have amplitudes (relative to the initial bleaching due to P*) of 21% and 14%, respectively. We also note that the yield of $P^+BPh_M^-$ appears to be slightly larger in KH versus H RCs (Table 4), indicating a consistent effect of the K mutation to enhance M-side electron transfer. Finally, the consistency in the arguments for M-side electron transfer also extends to the observation of the same 1−2 ns time constant for the KDH and DH RCs in all three key spectral regions (anion, P bleaching, and Q_X).

We consider next the decay pathways of $P^+BPh_M^-$; in other words, with what process is the 1−2 ns kinetic component associated? Clearly, the fact that there is P bleaching decay shows that the process being observed is charge recombination to the ground state rather than electron transfer to Q_B. This conclusion is independently mandated by the fact that the samples used in this study are devoid of Q_B (see Experimental Procedures). Also, we note that even if there were Q_B present, $P^+BPh_M^-$ → $P^+Q_B^-$ electron transfer would not give rise to P bleaching recovery, just as there is no recovery of the bleaching of P during $P^+BPh_L^-$ → $P^+Q_A^-$ electron transfer. Thus we assign the 1−2 ns kinetic component in the KDH and DH mutants as decay of $P^+BPh_M^-$ to the ground state. It is interesting to note that an inherent charge recombination time of 1−2 ns for $P^+BPh_M^-$ in these mutants is considerably shorter than the inherent charge recombination time of 10−20 ns for the L-side analogue $P^+BPh_L^-$ (measured in wt RCs in which Q_A is

removed or chemically prereduced). We will return to this point further below.

The 130−150 ps decay of P^+I^- on the L-side of the RC in the KDH and DH mutants is largely, we believe, associated with electron transfer to Q_A, although we cannot completely rule out a few percent yield of accompanying deactivation to the ground state. In our previous work on the DH mutant we noted that, under the model that $P^+BChl_L^-$ is at higher free energy in this mutant than in the H mutant, the intermediate P^+I^- is likely to reflect more the character of pure $P^+\beta^-$. Since mixing between these two states is thought to be the primary reason for the enhanced deactivation to the ground state in the H mutant relative to wt, it follows that the Asp at M201 tips the balance between ground-state deactivation and electron transfer to Q_A back to favoring the latter as indicated in Figure 2c,d. This effect is reflected in the shorter lifetime of P^+I^- in the KDH and DH mutants (130−150 ps) as compared to the H mutant (∼250 ps) and in the significantly different amounts of P bleaching recovery that accompany P^+I^- decay (∼25% in the H mutant compared to little if any in the KDH and DH mutants).

P Lifetimes and Rates and Yields of M-Side Electron Transfer*. We have shown here that putting a Lys 178 near $BChl_M$ appears to enhance electron transfer to the M branch. For the sake of discussion, it is useful to estimate the effect on the rate by application of a simple branching model for decay of P*. Let us assume the three pathways are P* → $P^+BPh_M^-$, P* → $P^+BPh_L^-$, and P* → ground state as in Figure 2d, with rate constants k_{PM}, k_{PL}, and k_{PG}, respectively. On the basis of the observed 15 ps P* lifetime and the yields given in Table 4 (e.g., 23% decay to $P^+BPh_M^-$ and so on), the calculated rate constants in the KDH mutant are $k_{PM} = (65\text{ ps})^{-1}$, $k_{PL} = (24\text{ ps})^{-1}$, and $k_{PG} = (100\text{ ps})^{-1}$. The same calculation for DH gives rate constants of $k_{PM} = (100\text{ ps})^{-1}$, $k_{PL} = (21\text{ ps})^{-1}$, and $k_{PG} = (100\text{ ps})^{-1}$. These estimates suggest, as one might initially expect, that the K mutation near $BChl_M$ predominantly modulates the rate of M-side electron transfer, causing it to be faster by roughly 50% in KDH compared to DH, and has little effect on the rates of deactivation to the ground state or electron transfer to the L-side.

Another similar exercise is to consider the effects induced by the K mutation on the P* lifetime. Let us assume that the L-side electron transfer and ground-state deactivation rates are unaffected by the K mutation and fix these rate constants at the calculated values for the DH mutant: $(21\text{ ps})^{-1}$ and $(100\text{ ps})^{-1}$, respectively. We then calculate that a $(58\text{ ps})^{-1}$ rate constant for electron transfer to the M-side is needed to give the measured 23% yield of $P^+BPh_M^-$ in the KDH mutant. Applying these three rate constants predicts a P* lifetime of 13.4 ps for the KDH mutant, which is within the error limits of the lifetime measured here (15 ± 2 ps). This calculation, based on a very simple model, is meant merely to demonstrate that a higher yield (and faster rate) of M-side electron transfer in the KDH versus DH mutants is not inconsistent with our finding the same P* lifetime within experimental uncertainty for the two RCs.

In the case of the KH mutant, the P* lifetime (8.5 ps) and $P^+BPh_M^-$ yield (∼10%) predict a value for the M-side rate constant of $k_{PM} \sim (85\text{ ps})^{-1}$, in good agreement with that of $(65\text{ ps})^{-1}$ estimated for KDH. And, similar to the above discussion, only a small difference in the P* lifetime would be predicted in going from the H to the KH mutant that would be beyond the signal to noise of our experiments to resolve with certainty. In the case of the other two K-containing RCs, KD and K, very low yields of M-side transfer (<10%) are predicted using similar analyses and the rate constants inferred from the data in Tables 2−4. However, for the KD and K mutants, as for other RCs with native pigment content, it is extremely difficult to discern low yields of M-side electron transfer from measurements such as those reported here. The small amplitudes of the BPh_M spectral signatures would be superimposed on the dominant signals due to the reduction of BPh_L, notably in the Q_X region. In this regard, if the value of $k_{PM} \sim (100\text{ ps})^{-1}$ obtained here and previously (*23*) by modeling the data for the DH mutant holds for wt RCs, then this implies a ratio of about 30/1 for L- versus the M-side initial charge separation in the native system. Comparable or larger lower limits for this ratio have been obtained previously (*55*, *58*).

Charge Recombination of $P^+BPh_M^-$ Compared to $P^+BPh_L^-$. Another new insight drawn from this study is that the inherent rate constant for $P^+BPh_M^-$ charge recombination to the ground state is on the order of $(1-2\text{ ns})^{-1}$ for both the KDH and DH mutants. This is roughly 10 times faster than the analogous $(10-20\text{ ns})^{-1}$ rate for $P^+BPh_L^-$ → ground state known for wt RCs depleted of Q_A or with Q_A prereduced. This difference represents another significant distinction between the two sides of the RC and has a number of interesting implications.

For one thing, an inherent $P^+BPh_M^-$ charge recombination rate of $(1-2\text{ ns})^{-1}$ would make it more difficult to support the same near quantitative yield of $P^+BPh_M^-$ → $P^+Q_B^-$ (when Q_B is present) as is found for $P^+BPh_L^-$ → $P^+Q_A^-$ on the L branch in wt RCs. For example, if M-side electron transfer to Q_B were to have the same $\sim(200\text{ ps})^{-1}$ rate constant as on the L-side, then a competing $P^+BPh_M^-$ → ground-state process with a rate constant of $(1\text{ ns})^{-1}$ would support an 83% yield of $P^+Q_B^-$ formation. Although this is a reasonably high yield, it is significantly less than the ∼100% yield on the L-side in the native RC. The $P^+Q_B^-$ yield would be reduced further still if the rate constant for electron transfer from $P^+BPh_M^-$ to Q_B were smaller than $(200\text{ ps})^{-1}$. We have been exploring M-side electron transfer to Q_B in collaboration with P. Laible and D. Hanson in Q_B-reconstituted mutants that contain DH plus another mutation near Q_A that prevents the RC from binding this cofactor. Preliminary measurements indicate a ≤10% yield of $P^+Q_B^-$ formed via the M-side in these RCs (*70*). On the basis of the experiments reported here, future studies will utilize the KDH template.

Why might $P^+BPh_M^-$ → ground-state charge recombination have a rate constant about 10-fold faster than that of $P^+BPh_L^-$ → ground state? In the simplest terms, the rate of a reaction is governed by electronic and Franck−Condon factors. The vibrational overlap factor involves the relationship between the free energy change (ΔG) and the pigment−protein reorganization energy (λ). One factor often considered for the relatively slow rate of charge recombination $P^+BPh_L^-$ → ground state (compared to the competing rate of charge separation $P^+BPh_L^-$ → $P^+Q_A^-$) is that the ΔG of about −1.1 eV is significantly larger than λ, placing the process in the Marcus inverted region (*9*, *35*, *71*). On this basis, one could initially speculate that the faster rate for the M-side process $P^+BPh_M^-$ → ground state could arise from a better Franck−Condon overlap if ΔG is smaller than for the L-side process

(and thus better matched to λ). However, the opposite may be the case. $P^+BPh_M^-$ appears to be at higher free energy than $P^+BPh_L^-$. This is thought to be due to the global effects of many amino acid residues that cause the M-side charge-separated states to be at somewhat higher free energy (by 0.1−0.3 eV) than their L-side counterparts (*43*−*48*). A major specific contributor is that BPh_M lacks a hydrogen bond analogous to the one BPh_L has between Glu L104 and its ring V keto group (*4*−*7*, *43*−*48*, *53*). Removal of this hydrogen bond makes the optical and vibrational properties of BPh_L more similar (but not identical) to those of BPh_M (*20*, *56*, *61*, *62*). Collectively, these factors suggest that $P^+BPh_M^-$ could be higher in free energy than $P^+BPh_L^-$ by $\gtrsim$0.1 eV (and thus below P* by $\lesssim$0.15 eV). Thus, if the values of λ for $P^+BPh_M^-$ and $P^+BPh_L^-$ charge recombination are similar (a point on which there is no direct information), the M-side process would have a poorer Franck−Condon factor and a slower rate, opposite to our observation.

The other factor to consider is the electronic contributions to the deactivation rates of $P^+BPh_M^-$ and $P^+BPh_L^-$. Spacial differences involving BPh_M, $BChl_M$, P, and the nearby protein residues versus the situation on the L-side will contribute to differences in the electronic couplings for M- versus L-side deactivation. Additionally, $P^+BPh_M^-$ charge recombination may involve mixing with either $P^+BChl_M^-$ or P*, as we have discussed previously for the L-side charge recombination reactions in beta-type and heterodimer mutants (*19*−*23*, *72*). Both of these states have inherently faster deactivation rates than $P^+BPh_M^-$ (due to larger electronic and/or other factors). In this regard, P* internal conversion has a rate of (100−300 ps)$^{-1}$ (*23*, *73*), and $P^+BChl_M^-$ charge recombination is expected to have a value on the order of (1 ns)$^{-1}$, based on analogy with $P^+BChl_L^-$.

Since $P^+BPh_M^-$ is almost certainly higher in free energy than $P^+BPh_L^-$, mixing with P* could facilitate deactivation of the M-side intermediate. However, it is equally or more plausible that the higher free energy of $P^+BPh_M^-$ results in a smaller energy gap and larger mixing between this state and $P^+BChl_M^-$ compared to that between $P^+BPh_L^-$ and $P^+BChl_L^-$. [Calculations vary by ±0.15 eV as to which gap is larger (*43*−*48*).] This would make the M-side of the RC analogous to the L-side mutants in which a small (free) energy gap between $P^+BPh_L^-/P^+\beta^-$ and $P^+BChl_L^-$ leads to an enhanced deactivation rate (Figure 2b). It cannot go unnoticed that the 1−2 ns deactivation time of $P^+BPh_M^-$ is comparable to the values of 0.6−1 ns obtained for the L-side intermediate in a number of beta-type RCs (*18*−*22*). Continuing this line of reasoning, the M-side charge recombination would be further enhanced by the extent to which $P^+BChl_M^-$ is stabilized by the incorporation of Lys L178 near $BChl_M$. In this regard, it is possible that $P^+BPh_M^-$ deactivation is actually somewhat faster in KDH versus DH RCs (though we are as yet unable to confirm this experimentally). Thus, the interesting dilemma arises that attempts to facilitate M-side electron transfer via stabilization of $P^+BChl_M^-$ could simultaneously, by bringing the two states closer in (free) energy, enhance subsequent charge recombination of $P^+BPh_M^-$. Of course, the latter effect could be compensated by stabilizing $P^+BPh_M^-$ via judicious changes in the amino acids near BPh_M.

If the analogy to the L-side β-containing mutants indeed holds, and $P^+BChl_M^-$ contributes to (or plays a dominant role in) driving the 1−2 ns charge recombination of $P^+BPh_M^-$, then these two states must be fairly close (likely within about 0.15 eV). This in turn means that $P^+BChl_M^-$ must lie close to both P* and $P^+BChl_L^-$ (since the latter state probably lies below P* as discussed above) and perhaps near the lower end of the 0.15−0.35 eV range of calculated (*43*−*48*) $P^+BChl_M^-$−$P^+BChl_L^-$ free energy gaps. If $P^+BChl_M^-$ lies slightly above P* and $P^+BChl_L^-$ slightly below in wild-type RCs, then the relative roles of the one- and two-step mechanisms to initial electron transfer along the two branches would be a straightforward and important determinant of directionality (*43*). If the closely spaced $P^+BChl_M^-$ and $P^+BChl_L^-$ *both* lie either below *or* above P* (depending on the mutant or in wild type), the observation of substantial directionality could imply a significant role of the electronic coupling between P* and $P^+BChl_L^-$ compared to that between P* and $P^+BChl_M^-$. Indeed, a number of calculations indicate that the L-side coupling is substantially larger than that on the M-side and that this difference makes a large contribution to directionality (*36*, *40*, *53*, *54*, *64*, *65*). Such a contribution would ultimately limit the effects on directionality that one could attain through shifting the free energies of the states on either branch individually or both branches simultaneously. These issues will be explored by further attempts to stabilize $P^+BChl_M^-$ to determine the ultimate effect on directionality.

In summary, we believe that, in addition to the demonstrated contribution of the free energies of $P^+BChl_M^-$ and $P^+BChl_L^-$ to directionality of charge separation, there are attractive aspects and implications of a role of differences in the electronic couplings on the L and M branches. Similarly, there is appeal and implications to the idea that $P^+BChl_M^-$ participates in the faster deactivation that is observed for $P^+BPh_M^-$ compared to $P^+BPh_L^-$. It is clear that the same unifying concepts that have emerged concerning the key roles of $P^+BChl_L^-$ and its free energy gap with other states in determining directionality, the mechanism of L-side initial electron transfer, and subsequent charge recombination processes must also hold for the M-side. Indeed, our findings and considerations indicate that we may be witnessing this fact in some of the mutants studied here. These concepts can be used to further manipulate the M-side processes to gain additional insights into the primary events.

ACKNOWLEDGMENT

We thank Drs. Richard Friesner and David Bocian for valuable discussions.

REFERENCES

1. Deisenhofer, J., and Norris, J. R., Eds. (1993) *The Photosynthetic Reaction Center*, Vol. II, Academic, San Diego.
2. Blankenship, R. E., Madigan, M. T., and Bauer, C. E., Eds. (1995) *Anoxygenic Photosynthetic Bacteria*, Kluwer Academic Publishers, Dordrect, The Netherlands.
3. Michel-Beyerle, M. E., Ed. (1996) *The Reaction Center of Photosynthetic Bacteria*, Springer, Berlin−Heidelberg.
4. Ermler, U., Fritzsch, G., Buchanan, S., and Michel, H. (1994) *Structure 2*, 925−936.
5. Deisenhofer, J., Epp, O., Sinning, I., and Michel, H. (1995) *J. Mol. Biol. 246*, 429−457.
6. Yeates, T. O., Komiya, H., Chirino, A., Rees, D. C., Allen, J. P., and Feher, G. (1988) *Proc. Natl. Acad. Sci. U.S.A. 85*, 7993−7997.

7. El-Kabbani, O., Chang, C.-H., Tiede, D., Norris, J., and Schiffer, M. (1991) *Biochemistry 30*, 5361−5369.
8. Bixon, M., Jortner, J., and Michel-Beyerle, M. E. (1991) *Biochim. Biophys. Acta 1056*, 301−315.
9. Bixon, M., Jortner, J., and Michel-Beyerle, M. E. (1995) *Chem. Phys. 197*, 389−404.
10. Nagarajan, V., Parson, W. W., Gaul, D., and Schenck, C. C. (1993) *Biochemistry 32*, 12324−12336.
11. Chan, C.-K., DiMagno, T. L., Chen, L. X.-Q., Norris, J. R., and Fleming, G. R. (1991*) Proc. Natl. Acad. Sci. U.S.A. 88*, 11202−11206.
12. Jia, Y., DiMagno, J., Chan, C.-K., Wang, Z., Du, M., Hanson, D. K., Schiffer, M., Norris, J. R., Fleming, G. R., and Popov, M. S. (1993) *J. Phys. Chem. 97*, 13180−13191.
13. Finkele, U., Lauterwasser, C., and Zinth, W. (1990) *Biochemistry 29*, 8517−8521.
14. Beekman, L. M. P., van Stokkum, I. H. M., Monshouwer, R., Rijnders, A. J., McGlynn, P., Visschers, R. W., Jones, M. R., and van Grondelle, R. (1996) *J. Phys. Chem. 100*, 7256−7268.
15. Shkurapatov, A. Y., and Shuvalov, V. A. (1993) *FEBS Lett. 322*, 168−172.
16. Schmidt, S., Arlt, T., Hamm, P., Huber, H., Nagele, T., Wachtveitl, J., Meyer, M., Scheer, H., and Zinth, W. (1994) *Chem. Phys. Lett. 223*, 116−120.
17. Huber, H., Meyer, M., Nagel, T., Hartl, I., Scheer, H., Zinth, W., and Wachtveitl, J. (1995) *Chem. Phys. 197*, 297−305.
18. Kennis, J. T. M., Shkuropatov, A. Y., van Stokkum, I. H. M., Gast, P., Hoff, A. J., Shuvalov, V. A., and Aartsma, T. J. (1997) *Biochemistry 36*, 16231−16238.
19. Kirmaier, C., Gaul, D., DeBey, R., Holten, D., and Schenck, C. C. (1991) *Science 251*, 922−927.
20. Kirmaier, C., Laporte, L., Schenck, C. C., and Holten, D. (1995) *J. Phys. Chem. 99*, 8910−8917.
21. Heller, B. A., Holten, D., and Kirmaier, C. (1995) *Biochemistry 34*, 5294−5302.
22. Heller, B. A., Holten, D., and Kirmaier, C. (1996) *Biochemistry 35*, 15418−15427.
23. Heller, B. A., Holten, D., and Kirmaier, C. (1995) *Science 269*, 940−945.
24. Holzwarth, A. R., and Müller, M. G. (1996) *Biochemistry 35*, 11820−11831.
25. Arlt, T., Dohse, B., Schmidt, S., Wachtveitl, J., Laussermair, E., Zinth, W., and Oesterhelt, D. (1996) *Biochemistry 35*, 9235−9244.
26. Volk, M., Aumeier, G., Langenbacher, T., Feick, R., Ogrodnik, A., and Michel-Beyerle, M. E. (1998) *J. Phys. Chem. B 102*, 735−751.
27. Vos, M. H., Rappaport, F., Lambry, J.-C., Breton, J., and Martin, J.-L. (1993) *Nature 363*, 320−325.
28. Small, G. J. (1995) *Chem. Phys. 197*, 239−257.
29. Stanley, R. J., and Boxer, S. G. (1995) *J. Phys. Chem. 99*, 859−863.
30. Zhou, H., and Boxer, S. G. (1998) *J. Phys. Chem. 102*, 9148−9160.
31. Lin, S., Taguchi, A. K. W., and Woodbury, N. W. (1996) *J. Phys. Chem. 100*, 17067−17078.
32. Haran, G., Wynne, K., Moser, C. C., Dutton, P. L., and Hochstrasser, P. L. (1996) *J. Phys. Chem. 100*, 5562−5569.
33. Marcus, R. A. (1987) *Chem. Phys. Lett. 133*, 471−477.
34. Almeida, R., and Marcus, R. A. (1990) *J. Phys. Chem. 94*, 2694−2701.
35. Warshel, A., Creighton, S., and Parson, W. W. (1988) *J. Phys. Chem. 92*, 2694−2701.
36. Scherer, P. O. J., and Fischer, S. F. (1989) *Chem. Phys. 131*, 115−127.
37. Skourtis, S. S., da Silva, A. J., Bialik, J. K., and Onuchic, J. N. (1992) *J. Phys. Chem. 96*, 8034−8041.
38. Hammerstad-Pedersen, J. M., Jensen, M. H., Khartkas, Y. I., Kznetsov, A. M., and Ulstrup, J. (1993) *Chem. Phys. Lett. 205*, 591−576.
39. Sim, E., and Makri, N. (1997) *J. Phys. Chem. B 101*, 5446−5438.
40. Zhang, L. Y., and Friesner, R. A. (1998) *Proc. Natl. Acad. Sci. U.S.A. 95*, 13603−13605.
41. Gunner, M. (1991) *Curr. Top. Bioenerg. 16*, 319.
42. Peloquin, J. M., Williams, J. C., Lin, X., Alden, R. G., Taguchi, A. K. W., Allen, J. P., and Woodbury, N. W. (1994) *Biochemistry 33*, 8089−8100.
43. Parson, W. W., Chu, Z.-T., and Warshel, A. (1990) *Biochim. Biophys. Acta 1017*, 251−272.
44. Alden, R. G., Parson, W. W., Chu, Z. T., and Warshel, A. (1995) *J. Am. Chem. Soc. 117*, 12284−12298.
45. Thompson, M. A., Zerner, M. C., and Fajer, J. (1991) *J. Am. Chem. Soc. 113*, 8210−8215.
46. Marchi, M., Gehlen, J. N., Chandler, D., and Newton, M. (1994) *Science 263*, 499−502.
47. Gunner, M. R., Nicholls, A., and Honig, B. (1996) *J. Phys. Chem. 100*, 4277−4291.
48. Blomberg, M. R. A., Siegbahn, P. E. M., and Babcock, G. T. (1998) *J. Am. Chem. Soc. 120*, 8812−8824.
49. Fajer, J., Brune, D. C., Davis, M. S., Forman, A., and Spaulding, L. (1975) *Proc. Natl. Acad. Sci. U.S.A. 72*, 4956−4960.
50. Cua, A., Kirmaier, C., Holten, D., and Bocian, D. F. (1998) *Biochemistry 37*, 6394−6401.
51. Williams, J. C., Alden, R. H., Murchison, H. A., Peloquin, J. M., Woodbury, N. W., and Allen, J. P. (1992) *Biochemistry 31*, 11029−11037.
52. Czarnecki, K., Kirmaier, C., Holten, D., and Bocian, D. F. (1999) *J. Phys. Chem. A 103*, 2235−2246.
53. Michel-Beyerle, M. E., Plato, M., Deisenhofer, J., Michel, H., Bixon, M., and Jortner, J. (1988) *Biochim. Biophys. Acta 932*, 52−70.
54. Plato, M., Möbius, K., Michel-Beyerle, M. E., Bixon, M., and Jortner, J. (1988) *J. Am. Chem. Soc. 110*, 7279−7285.
55. Bixon, M., Jortner, J., Michel-Beyerle, M. E., and Ogrodnik, A. (1989) *Biochim. Biophys. Acta 977*, 273−286.
56. Bylina, E. J., Kirmaier, C., McDowell, L. M., Holten, D., and Youvan, D. C. (1988) *Nature 336*, 182−184.
57. Deleted in revision.
58. Kellogg, E. C., Kolaczkowski, S., Wasiewlewski, M. R., and Tiede, D. M. (1989) *Photosynth. Res. 22*, 47−59.
59. McDowell, L. M., Gaul, D., Kirmaier, C., Holten, D., and Schenck, C. C. (1991) *Biochemistry 30*, 8315−8322.
60. Steffen, M. A., Lao, K., and Boxer S. G. (1994) *Science 264*, 810−816.
61. Palaniappan, V., and Bocian, D. F. (1995) *J. Am. Chem. Soc. 117*, 3647−3448.
62. Peloquin, J. M., Bylina, E. J., Youvan, D. C., and Bocian, D. F. (1991) *Biochim. Biophys. Acta 1056*, 85−88.
63. Lin, S., Xiao, W., Eastman, J. E., Taguchi, A. K. W., and Woodbury, N. W. (1996) *Biochemistry 35*, 3181−3196.
64. Ivashin, N., Kallenbring, B., Larsson, S., and Hansson, O. (1998) *J. Phys. Chem. B 102*, 5017−5022.
65. Hasegawa, J., and Nakatsuji, H. (1998) *J. Phys. Chem. B 102*, 10420−10439.
66. Bylina, E. J., and Youvan, D. C. (1988) *Proc. Natl. Acad. Sci. U.S.A. 85*, 7226−7230.
67. Brudvig, G. W., Worland, S. T., and Sauer, K. (1983) *Proc. Natl. Acad. Sci. U.S.A. 80*, 683−686.
68. Kirmaier, C., and Holten, D. (1991) *Biochemistry 30*, 609−613.
69. Robert, B., Tiede, D. M., and Lutz, D. M. (1985) *FEBS Lett. 183*, 326−330.
70. Laible, P. D., Kirmaier, C., Holten, D., Tiede, D. M., Schiffer, M., and Hanson, D. K. (1998) in *Photosynthesis: Mechanisms and Effects* (Garab, G., Ed.) pp 849−852, Kluwer, Dordrecht.
71. Marcus, R. A., and Sutin, N. (1985) *Biochim. Biophys. Acta 81*, 265.
72. Laporte, L., McDowell, L. M., Kirmaier, C., Schenck, C. C., and Holten, D. (1993) *Chem. Phys. 176*, 615−629.
73. Breton, J., Martin, J.-L., Lambry, S., Robles, D., and Youvan, C. (1990) in *Reaction Centers of Photosynthetic Bacteria* (Michel-Beyerle, M. E., Ed.) Springer Series in Biophysics, Part 6, p 293, Springer, New York.

BI9908585